

Baselines for higher-order cumulants of net-charge distributions from balance function

Igor Altsybeev^{1,*}

¹*Saint-Petersburg State University, 7/9 Universitetskaya nab., St. Petersburg, 199034 Russia*
(Dated: February 27, 2020)

In studies of heavy-ion collisions, fluctuations of conserved quantities are considered as an important signal of the transition between the hadronic and partonic phases of matter. In this paper, connection between the balance function and several integrated observables used in studies of net-charge fluctuations is discussed. It is highlighted that a difference between balance function definitions used in various experiments has implications on its physical meaning and on the interpretation of balance function integrals as well, for that, several illustrative models are considered. In the second half of the paper, simple expressions for higher-order cumulants of net-charge distribution are derived under the assumption that particle-antiparticle pairs are produced in local processes from sources that are nearly uncorrelated in rapidity. For calculations with these expressions, one needs to know only the balance function integral and low-order cumulants of particle number distribution measured within an experimental acceptance. Values estimated in such a way could be considered as baselines for direct measurements of higher-order net-charge fluctuations.

I. INTRODUCTION

Heavy-ion collisions at relativistic energies allow investigating properties of nuclear matter at extreme conditions. One of the key theoretical predictions confirmed by LQCD calculations [1] is that at high energy densities, reached at RHIC and LHC, nuclear matter transforms into a deconfined state of quarks and gluons known as Quark-Gluon Plasma (QGP). As a possible signature of the transition between the hadronic and partonic phases, it is theoretically shown that higher-order fluctuations of conserved quantities, such as net-charge, net-baryon, net-strangeness, should greatly enhance near the critical point [2]. At LHC energies, a temperature-driven second order phase transition between a hadron gas and the QGP is expected [3].

A number of observables are used to study the net-charge fluctuations. Among them are charge balance functions [4] that allow studying in a differential way the separation of the opposite charges in a momentum space. The balance functions have been extensively studied in experiments [5–9]. There are also integrated quantities expressed via moments of net-charge distributions of particles registered within an experimental acceptance. The second moment of net-charge distribution is often studied in terms of the ν_{dyn} quantity introduced in [10], and there is a plenty of experimental results based on this observable [11–13]. Alternatively, the ratio of the second moment to average numbers of protons and antiprotons could be measured, see, for instance, recent ALICE results on net-proton [14] and net- Λ [15] fluctuations. The higher moments of net-charge distributions are extensively studied as well [16], in particular, the STAR collaboration reported the energy dependence of net-proton [17] as well as net-kaon [18] number fluctuations in terms

of cumulants up to the fourth order. Net-proton and net-kaon fluctuations are usually considered as a proxy for the net-baryon and net-strangeness, respectively.

There are mathematical connections between observables mentioned above. In particular, the balance function could be integrated over available pair separation range and in this way be connected to the ν_{dyn} observable [6, 10, 19], as well as to the second moment of net-charge distribution [20]. There are caveats, however, in details of how this integration is being performed. This is discussed in Section II of the current paper.

Mentioned observables possess different sensitivity to various physical processes. For example, cumulants of particle distributions, starting already from the second-order cumulant, are sensitive to fluctuations in number of emitting sources – the so-called “volume fluctuations”, discussed, for instance, in [21, 22], which makes interpretation of the experimental measurements highly non-trivial, especially for higher-order cumulants. On the other hand, the second-order observable ν_{dyn} is robust to volume fluctuations (under the assumption that the sources are independent).

It should be mentioned also, that there are charge conservation laws that influence the net-charge distributions measured within some (limited) experimental acceptance. One may distinguish *global* conservation laws, which should obviously be fulfilled in each collision as a whole, and *local* conservation laws, which lead to production of particle pairs with opposite charges that are close in space. The conservation laws should be taken into account when one tries to extract signals of critical behaviour from measured observables [21, 23, 24].

Both volume fluctuations and conservation laws lead to the need of some solid baselines for experimentally measured values of the higher-order cumulants. In the present paper, the baselines for higher-order cumulants of net-charge distributions at LHC energies are derived under the assumption that oppositely charged particle pairs in each event are produced in independent local processes

* e-mail: i.altsybeev@spbu.ru

from sources that are loosely correlated in rapidity. This allows reducing expressions for higher-order cumulants, so that only the second cumulant of net-charge distribution and several low-order cumulants of positive (or negative) particle number distribution are required for calculations. In turn, the net-charge second order cumulant may be expressed via the balance function integral.

The paper organized as follows. In Section II, a connection between the ν_{dyn} and the balance function at LHC energies is recollected, a notion of the balance function integral is clarified, and differences in physics interpretation of these quantities are discussed. The case of multiple types of emitting sources is also considered. In Section III, connection between the second cumulant of net-charge distribution and the balance function is recalled. The main part of the paper is Section IV, where expressions for higher-order cumulants of net-charge distributions are derived under the assumption of local production of charge pairs mentioned above. These expressions are then applied to simple models as well as to events from monte-carlo generators in order to compare with cumulants calculated directly. After that, basing on available ALICE data, a predictions for forth-to-second cumulant ratio is done for Pb-Pb collisions. In Appendix, formulae for cumulants of particle distribution in a system with fluctuating number of emitting sources are provided up to the 8th order.

II. ν_{dyn} AND BALANCE FUNCTION

A. Definitions

When particles of the two species A and B are registered within experimental acceptance Y , event-by-event fluctuations of their relative yields are often studied using quantity ν_{dyn}^{AB} suggested in [10] and defined in terms of moments of particle multiplicity distributions as

$$\nu_{dyn}^{AB} = \frac{\langle N_A(N_A - 1) \rangle}{\langle N_A \rangle^2} + \frac{\langle N_B(N_B - 1) \rangle}{\langle N_B \rangle^2} - 2 \frac{\langle N_A N_B \rangle}{\langle N_A \rangle \langle N_B \rangle}, \quad (1)$$

where N_A and N_B are the multiplicities of particles A and B in a single event and angular brackets denote averaging over all events. A and B may mean different particle species (for example, pions and kaons) or just sign of particle electric charge. The ν_{dyn} has been studied in a number of experiments, in particular, in analysis of Pb-Pb collisions in ALICE it was used as a measure of net-charge fluctuations [12], fluctuations of relative particle yields K/π , p/π and K/p [13] as well as for fluctuations of net-protons [14].

One of the notable properties of the ν_{dyn} is that in models with independent identical particle sources it does not depend on fluctuations of number of sources (volume fluctuations). However, it still depends on an average number of sources $\langle N_S \rangle$, namely, scales inversely with it:

$$\nu_{dyn}^{AB} = \frac{1}{\langle N_S \rangle} \tilde{\nu}_{dyn}^{AB}, \quad (2)$$

where $\tilde{\nu}_{dyn}^{AB}$ characterizes the fluctuations for a single source. Denoting multiplicities from a single source as n_A and n_B , we have $\langle N_A \rangle = \langle n_A \rangle \langle N_S \rangle$ and $\langle N_B \rangle = \langle n_B \rangle \langle N_S \rangle$, and the $1/\langle N_S \rangle$ scaling could be eliminated, for example, by introducing the following observable:

$$\nu_s^{AB} \equiv \frac{-\nu_{dyn}^{AB}}{1/\langle N_A \rangle + 1/\langle N_B \rangle} = \frac{-\tilde{\nu}_{dyn}^{AB}}{1/\langle n_A \rangle + 1/\langle n_B \rangle}, \quad (3)$$

where the subscript s implies ‘‘scaled’’. Quantities that depend neither on $\langle N_S \rangle$ nor on event-by-event fluctuations of N_S are usually referred to as strongly-intensive observables, and the scaled quantity ν_s^{AB} belongs to this class of measures. In fact, ν_s^{AB} is closely related to the Σ^{AB} observable introduced in [25], the connection between the two reads as $\nu_s^{AB} = 1 - \Sigma^{AB}$.

Let the symbols A and B denote the electric charge. At LHC energies at mid-rapidity, numbers of positive and negative particles are on average the same, so that $\langle N^+ \rangle = \langle N^- \rangle$ and $\langle N^+ N^+ \rangle = \langle N^- N^- \rangle$, thus ν_s^{AB} (3) can be rewritten as

$$\nu_s^{+-} = -\frac{\langle N^+ \rangle}{2} \nu_{dyn}^{+-} = \frac{\langle N^+ N^- \rangle - \langle N^+ (N^+ - 1) \rangle}{\langle N^+ \rangle}. \quad (4)$$

Note that at the LHC energies the same expression (4) holds not only for electric charges, but also for baryon-antibaryon and strange-antistrange particle pairs. Below, the superscript in ν_s^{+-} will be omitted.

If a system consists of (possibly correlated) sources and each source emits a pair of oppositely charged particles (so that produced particles do not interact in any charge-dependent way with the rest of the system), the minus sign in the numerator of (3) allows turning the values of ν_s to be positive and thus to acquire a meaningful interpretation for the values of ν_s (4): under assumptions mentioned above, it provides a conditional probability for a particle, registered within an experimental acceptance, to observe an oppositely charged partner within the same acceptance. This clear physical meaning of ν_s makes it preferable to the Σ observable. Note, however, that ν_s in principle may have negative values in case if significant final state correlations between same-charged particles are present [12].

Another handy observable used in studies of heavy-ion collisions is the balance function (BF) that was proposed as a convenient measure of the resulting correlations between the opposite charges in the momentum space [4]. Balance function at some (pseudo)rapidity gap $\Delta y = y_1 - y_2$ between two particles, detected at rapidities y_1 and y_2 , is defined through the single-particle densities

$\rho_1(y)$ and two-particle densities $\rho_2(y_1, y_2)$ as follows:

$$B(\Delta y) = \frac{1}{2} \left[\frac{\rho_2^{+-}(\Delta y)}{\rho_1^+(y_1)} + \frac{\rho_2^{-+}(\Delta y)}{\rho_1^-(y_1)} - \frac{\rho_2^{++}(\Delta y)}{\rho_1^+(y_1)} - \frac{\rho_2^{--}(\Delta y)}{\rho_1^-(y_1)} \right], \quad (5)$$

where superscripts $+$ and $-$ denote signs of particle electric charges (the strangeness or baryonic charges may be considered as well). The BF was extensively measured in experiments, see, for instance, [5, 7, 8]. At LHC energies at mid-rapidity, we may put $\rho_1^+ = \rho_1^-$ at all y , and $\rho_2^{++} = \rho_2^{--}$ at each Δy , thus, (5) simplifies to

$$B(\Delta y) = \frac{\rho_2^{+-}(\Delta y) - \rho_2^{++}(\Delta y)}{\rho_1^+}. \quad (6)$$

In the model with particle sources, the balance function does not depend on an average number of sources in a system, as well as on source number fluctuations (i.e. it's a strongly intensive observable, similarly to ν_s). Note that this holds also for the case when multiple types of *charge-neutral* sources are present in a system and relative fractions of source numbers are fixed on average. In this case, a BF that is a ‘‘weighted average’’ over sources could be considered, this is discussed later in Section II D. If each source decays into a pair of opposite charges, the balance function (5) has a meaning of a conditional probability density for a given particle to have an oppositely charged partner at a gap Δy [4]. However, similarly to what was noted about the ν_s observable above, this interpretation does not hold if there are charge-dependent correlations between the produced particles, for example, due to HBT effects.

In case when particle registration efficiency is a constant in a considered kinematic range, both ν_s and $B(\Delta y)$ can be trivially corrected for the efficiency, since correction is needed only for the first moments of particle numbers.

B. Connection between observables

In addition to $B(\Delta y)$, one may also consider a balance function between particular rapidity points y_1 and y_2 :

$$B(y_1, y_2) = \frac{1}{2} \left[\frac{\rho_2^{+-}(y_1, y_2)}{\rho_1^+(y_1)} + \frac{\rho_2^{-+}(y_1, y_2)}{\rho_1^-(y_1)} - \frac{\rho_2^{++}(y_1, y_2)}{\rho_1^+(y_1)} - \frac{\rho_2^{--}(y_1, y_2)}{\rho_1^-(y_1)} \right]. \quad (7)$$

In an experiment with the rapidity acceptance Y , in order to get $B(\Delta y)$ as a function of the gap Δy , one typically does the following integration of (7):

$$B(\Delta y) = \frac{1}{\Omega(\Delta y)} \int_{-Y/2}^{Y/2} \int_{-Y/2}^{Y/2} \int_{\Omega} B(y_1, y_2) \delta(\Delta y - y_1 + y_2) \delta(\bar{y} - (y_1 + y_2)/2) dy_1 dy_2 d\bar{y}, \quad (8)$$

where $\Omega(\Delta y) = Y - \Delta y$ is the so-called *acceptance correction factor* that represents the width of the acceptance in $\bar{y} = (y_1 + y_2)/2$ at a given $\Delta y = y_1 - y_2$ [9]. This correction implies that the $B(\Delta y)$ for a given separation Δy is obtained by averaging over all possible positions \bar{y} of the middle between the two particles. Results obtained with the event-mixing technique [6, 7] are corrected for the size of the acceptance as well, since division by a mixed-events pair distribution effectively corresponds to division by the factor $\Omega(\Delta y)$ (see also [26]).

We may also introduce the integral of the balance function:

$$I_{BF} = \int_{-Y}^Y B(\Delta y) d(\Delta y), \quad (9)$$

where the limits correspond to maximum separation between the particles within the acceptance¹. In the model of emitters that produce oppositely-charged particle pairs, the integral (9) can be interpreted as a probability for a particle to have an oppositely charged partner at y -separation range from $-Y$ to Y . We will see in Section II C, however, that there could be caveats in such an interpretation at certain conditions.

Definitions (8) of the balance function and (9) of its integral are adopted in ALICE collaboration (see [6–9]), and, because of the acceptance correction, they allow interpretation in terms of probability of separation distance Δy between the opposite charges, irrespective of the acceptance of a detector used for the study. However, the balance function may be defined also in a different way, namely, without the division by the $\Omega(\Delta y)$ factor in (8) [10, 19]. In this case, the physics interpretation of the balance function changes, namely, such a BF can be interpreted as a probability density for a given particle to observe an oppositely charged partner *within the experimental acceptance*, consequently, it depends on the acceptance width Y . This definition is used, for instance, in STAR collaboration (in particular, in [5]). It is crucial to realize the difference between these two definitions of BF when one compares experimental results from different collaborations, as it is emphasized, for instance, in [6].

We may integrate $B(y_1, y_2)$ (7) over Y directly. At LHC energies, $\langle N^+ \rangle = \langle N^- \rangle$ and the translational invariance within the acceptance Y is assumed, so the integration gives

$$\begin{aligned} & \int_{-Y/2}^{Y/2} \int_{-Y/2}^{Y/2} B(y_1, y_2) dy_1 dy_2 = \\ & = \frac{Y}{\langle N^+ \rangle} \left[\langle N^+ N^- \rangle - \langle N^+ (N^+ - 1) \rangle \right] = Y \nu_s, \quad (10) \end{aligned}$$

¹ When one plots experimental data for the $B(\Delta y)$, the sign of Δy is usually taken into account, so that the $B(\Delta y)$ is drawn symmetrically with respect to $\Delta y = 0$.

where $\rho_1^+(y)$ is rewritten as $\langle N^+ \rangle / Y$. Using (8) and (10), it is now straightforward to express ν_s as a *weighted* integral of $B(\Delta y)$:

$$\nu_s = \int_{-Y}^Y B(\Delta y) \left(1 - \frac{|\Delta y|}{Y}\right) d(\Delta y). \quad (11)$$

As it was discussed in the previous section, under certain conditions the ν_s can be interpreted as a probability for a registered particle to observe an oppositely charged partner *within acceptance* Y . This interpretation differs from the interpretation of the integral I_{BF} defined by (9).

Thus, we got two integrals of the balance function – I_{BF} (9) and ν_s (11) – that have different meanings. The connection between the two may be written as

$$\nu_s = I_{BF} - \frac{2}{Y} \int_0^Y B(\Delta y) \Delta y d(\Delta y). \quad (12)$$

Similarly what was said about balance functions above, when one mentions a balance function integral, it is important to clarify explicitly which of the two definitions is being discussed. Note also, that if $B(\Delta y)$ as a function of Δy is available from an experiment, one may readily calculate both ν_s and I_{BF} . In the following text, the definition of balance function (8) *with* acceptance correction will be used by default.

C. Specific cases

Consider the case when particles are 100% detectable once they appear within the acceptance Y . In models with particle-antiparticle pair sources, from (12) it immediately follows that $\nu_s = I_{BF} = 1$ only for an infinitely narrow balance function (i.e. when the gap Δy between the correlated opposite-sign charges is always zero), and

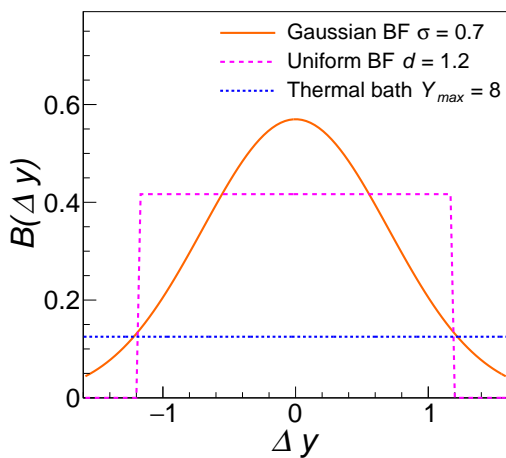


FIG. 1. Balance functions with Gaussian ($\sigma = 0.7$, solid line), uniform (width $d = 1.2$, dashed line) shapes. Dotted line shows the BF for the “thermal bath” model. Experimental acceptance $Y = 1.6$.

$\nu_s < I_{BF}$ in other cases. As another extreme, one can imagine the case when correlated opposite charge pairs are always separated by a gap $|\Delta y| = (Y - \delta)$ with $\delta \rightarrow 0$, so that the gap is slightly less than the acceptance width Y – in this case, $I_{BF} = 1$, while $\nu_s \rightarrow 0$.

Now, let us consider three more instructive models of pair emission that allow analytical calculations. The first two models specify $B(\Delta y)$ for each particle source, while the distribution of the sources is flat in a wide rapidity range $\gg Y$. The third model implies complete “thermalization” of the charges within some rapidity range Y_{\max} .
(i) Gaussian balance function $B(\Delta y) = \frac{1}{\sqrt{2\pi}\sigma} e^{-\Delta y^2/2\sigma^2}$ (solid line in Figure 1). Expressions (9) and (11) give

$$I_{BF} = \text{erf}\left(\frac{Y}{\sqrt{2}\sigma}\right), \quad \nu_s = \text{erf}\left(\frac{Y}{\sqrt{2}\sigma}\right) - \sqrt{\frac{2}{\pi}} \frac{\sigma}{Y} \left(1 - e^{-\frac{Y^2}{2\sigma^2}}\right). \quad (13)$$

Dependences of these quantities on the experimental acceptance Y for the case when $\sigma = 0.7$ are shown in Figure 2 (a). Circles denote values calculated in a corresponding toy monte-carlo model. Bottom panel shows the ratio

$$\nu_s/I_{BF} = 1 - \sqrt{\frac{2}{\pi}} \frac{\sigma}{Y} \left(1 - e^{-\frac{Y^2}{2\sigma^2}}\right) / \text{erf}\left(\frac{Y}{\sqrt{2}\sigma}\right). \quad (14)$$

Within sufficiently large acceptance $Y \gtrsim 3\sigma$, the I_{BF} comes very close to unity, while ν_s approaches the unity slower.

(ii) A somewhat more artificial case is the balance function that is uniform within $|\Delta y| \leq d$ and has a constant value $B(\Delta y) = \frac{1}{2d}$, while it’s zero at $|\Delta y| > d$ (dashed line in Figure 1). The I_{BF} and ν_s for this case (Figure 2, b) are

$$I_{BF} = \begin{cases} \frac{Y}{d}, & Y \leq d \\ 1, & Y > d \end{cases}, \quad \nu_s = \begin{cases} \frac{Y}{2d}, & Y \leq d \\ 1 - \frac{d}{2Y}, & Y > d \end{cases}, \quad (15)$$

and the ratio is

$$\nu_s/I_{BF} = \begin{cases} \frac{1}{2}, & Y \leq d \\ 1 - \frac{d}{2Y}, & Y > d \end{cases}. \quad (16)$$

In this model (ii), the BF integral reaches unity as soon as the Y acceptance is large enough to cover the range of possible particle separations, while the ν_s reaches unity only at $Y \rightarrow \infty$.

(iii) One may consider a model where in each event positive and negative particles are produced in pairs, but then the particle rapidities are “thermalized”, i.e. distributed uniformly within some range Y_{\max} (a “thermal bath”), while the measurements are done in an acceptance $Y \in Y_{\max}$. In this model, the $B(\Delta y)$, measured within acceptance Y , equals $1/Y_{\max}$ at all Δy , and

$$I_{BF} = \frac{2Y}{Y_{\max}}, \quad \nu_s = \frac{Y}{Y_{\max}}. \quad (17)$$

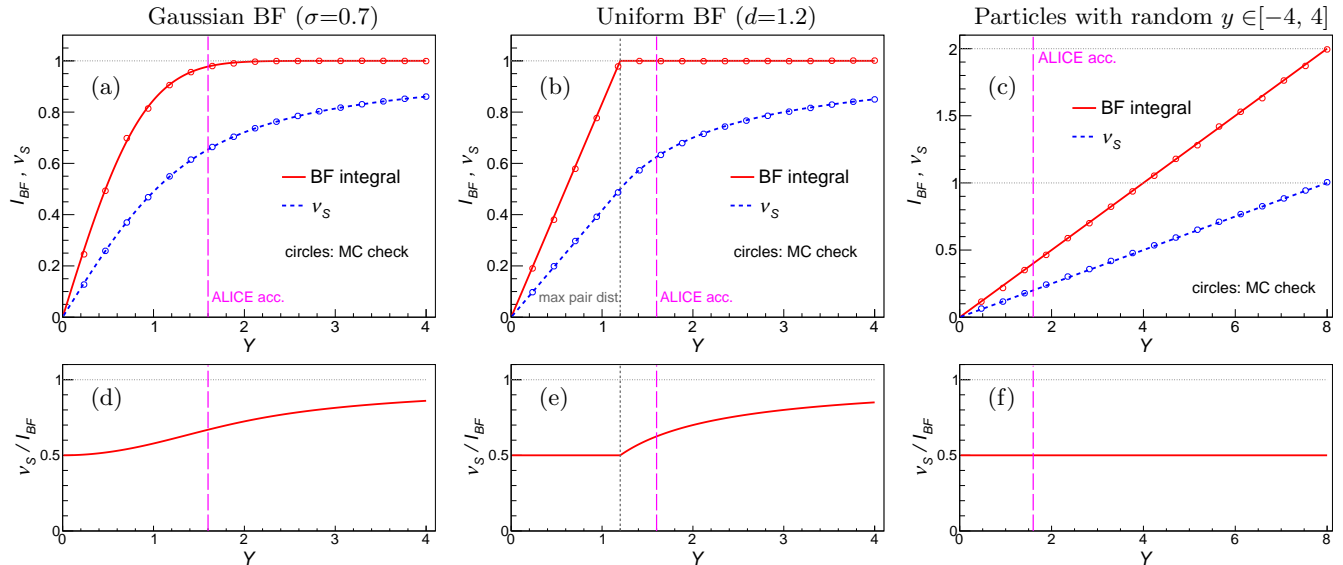


FIG. 2. Dependence of the balance function integral (solid lines) and the ν_s (dashed lines) on the experimental acceptance width Y : (a) – for Gaussian BF (with $\sigma = 0.7$), (b) – for BF that is uniform at gaps up to $d = 1.2$ units, (c) – in case of particles randomly distributed in a range $y \in [-4, 4]$. Circles show calculations in a toy monte-carlo model for the cross-check. Bottom panels show corresponding ν_s/I_{BF} ratios. To guide the eye, a vertical dashed line in magenta indicates the η -acceptance of the ALICE detector.

In particular, when $Y = Y_{\max}$, the I_{BF} reaches value 2. Figure 2 (c) shows the I_{BF} and ν_s in this model as a function of Y for the case when $Y_{\max} = 8$, namely, when particles are randomly distributed within $y \in [-4, 4]$.

It may be noticed, that the interpretation of the BF integral I_{BF} (9) as a conditional probability fails for the thermal model (iii), and the values may go beyond 1. The origin of the fact that the BF integral I_{BF} exceeds unity is in a subtle detail of the model (iii): the probability for a particle, observed at some y , to have an oppositely charged partner at a gap Δy is not the same as to find it at $-\Delta y$ (this “asymmetry” is introduced by “thermalization” of the particle rapidities within the rigid global boundaries of the system in this model). In this case, the boost-invariance condition for $B(\Delta y)$ is violated, while this condition is essential for treatment of the BF integral as a conditional probability. At the same time, interpretation of ν_s as a probability of finding a balancing charge within the acceptance Y holds.

D. Composition of sources

It is instructive to get explicit expressions for observables ν_s and $B(\Delta y)$ for the case when *charge-neutral* sources of multiple types are present in the system. We may consider, for example, a system with neutral resonances like ρ^0 and ω , quark-gluon strings (if they are long enough in rapidity so that charges at the string ends do not play a role), etc. If there are M_s different types of neutral sources (the sources may be correlated) with known balance functions $B^i(\Delta y)$ for each type, the over-

all balance function can be constructed [27] as a sum

$$B(\Delta y) = \sum_{i=1}^{M_s} \alpha^i B^i(\Delta y), \quad (18)$$

where α^i are weights defined as

$$\alpha^i = \frac{\langle N^i \rangle}{\sum_{i=1}^{M_s} \langle N^i \rangle}. \quad (19)$$

Here, $\langle N^i \rangle$ is an average number of particles from all sources of i -th type. If each source decays into a pair of oppositely charged particles, expression (18) decomposes a probability for a given particle to observe an oppositely charged partner at gap Δy as a sum of products of (a) fraction of particles emitted from sources of i -th type and (b) probability for this source type to have a separation Δy between the produced charges.

Integration of (18) over Δy gives a “decomposition” for the BF integral (9):

$$I_{BF} = \sum_{i=1}^{M_s} \alpha^i I_{BF}^i, \quad (20)$$

while integration using (11) gives a decomposition for ν_s :

$$\nu_s = \sum_{i=1}^{M_s} \alpha^i \nu_s^i. \quad (21)$$

The last result is similar to formula (38) in [26] (see also [28]), which was derived in terms of the Σ observable for the model with superposition of strings of different types.

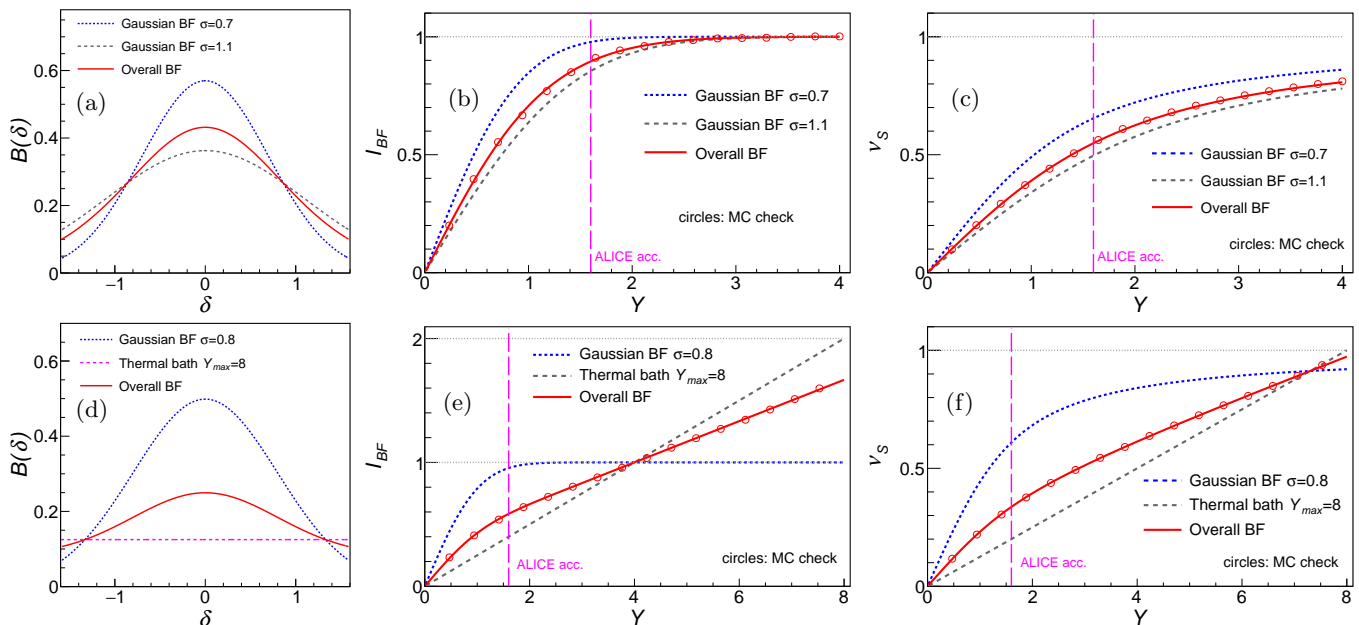


FIG. 3. Balance function (a, d), BF integral (b, e) and ν_s (c, f) in events with two types of particle pair sources. Weighted sums calculated with (18), (20) and (21) are drawn as solid red lines. Top row: 1/3 of all particles are from sources with Gaussian BF with $\sigma = 0.7$, 2/3 of particles – from Gaussian sources with $\sigma = 1.1$. Bottom row: 1/3 of particles are from Gaussian sources with $\sigma = 0.8$ and 2/3 are particle pairs that are “thermalized” within $Y_{\max} = 8$ rapidity range. Circles show calculations in a toy monte-carlo model.

For illustrative purposes, model calculations of $B(\Delta y)$, I_{BF} and ν_s with two distinct types of particle-antiparticle sources are shown in Figure 3. In model shown in the first row, 1/3 of all the sources (on average) have Gaussian balance function with width $\sigma_1 = 0.7$, other 2/3 of the sources also have Gaussian BF, but with $\sigma_2 = 1.1$. In the second row, 1/3 of the sources (on average) have Gaussian BF with $\sigma = 0.8$ and 2/3 – thermal BF within the range $Y_{\max} = 8$. Calculations for source superpositions, done using (18), (20) and (21), are plotted as solid lines. The possibility of such decompositions preserves the probabilistic interpretation of the observables in a much wider range of models and is useful to be kept in mind.

III. CONNECTION BETWEEN BALANCE FUNCTION AND SECOND CUMULANT OF NET-CHARGE DISTRIBUTION

The second cumulant of net-charge distribution is defined by

$$\kappa_2(\Delta N) = \langle (\Delta N)^2 \rangle - \langle \Delta N \rangle^2, \quad (22)$$

where $\Delta N = N^+ - N^-$ is the difference between numbers of particles of opposite charges, measured within the Y rapidity acceptance in a given event. When distribution of each of these numbers is Poissonian, their difference has the so called Skellam distribution, with cumulants $\kappa_r(\Delta N) = \langle N^+ \rangle + (-1)^r \langle N^- \rangle$, $r = 1, 2, \dots$ [21]. The

Poissonian particle production is usually considered as a baseline model, so it is helpful to define the ratio of the $\kappa_2(\Delta N)$ to the second cumulant of the Skellam distribution

$$r_{\Delta N} = \frac{\kappa_2(\Delta N_p)}{\langle N^+ \rangle + \langle N^- \rangle}, \quad (23)$$

which is used in experimental studies [14]. In [20], it was shown that at the LHC energies the ratio $r_{\Delta N}$ is connected to the ν_{dyn} observable by the following expression:

$$1 - r_{\Delta N} = -\frac{\langle N^+ \rangle}{2} \nu_{dyn}^{+-}. \quad (24)$$

It is also claimed in [20] that the quantity on the RHS of (24) is equal to the integral of the balance function. It should be noted, however, that this connection is valid only if the balance function is defined as in STAR [5], namely, if it is *not* corrected for the acceptance factor $\Omega(\Delta y)$, discussed in Section II, while such a correction is typically performed in ALICE [6, 7]. Indeed, the RHS of (24) is actually the ν_s observable, defined by (4), and we can rewrite expression (24) as

$$r_{\Delta N} = 1 - \nu_s, \quad (25)$$

where ν_s itself can be evaluated with (11), provided the balance function of the system is known:

$$r_{\Delta N} = \frac{\kappa_2(\Delta N_p)}{\langle N^+ \rangle + \langle N^- \rangle} = 1 - \int_{-Y}^Y B(\Delta y) \left(1 - \frac{|\Delta y|}{Y}\right) d\Delta y. \quad (26)$$

Thus, if the BF of the system is measured, one can readily calculate the cumulant ratio via (26). After establishing this connection between the balance function and the cumulant ratio, we may now plot the dependence of the $r_{\Delta N}$ on acceptance Y for the three models of balance function (i)-(iii), discussed in the previous section. These dependences are shown in Figure 4. Calculations are done analytically, by substituting ν_s from (13), (15) and (17) into (25).

When the numbers N^+ and N^- are treated as numbers of baryons and antibaryons in the system, so that ΔN is a baryonic net-charge, we may note that the model (iii) of the “thermal bath”, discussed in the previous section, is equivalent to the model of *global* baryon number conservation considered in [21] (in this case, Y_{\max} corresponds to 4π acceptance). Next, the BF model (ii) is similar to the model with baryon-antibaryon pairs, considered numerically in [24], where distance between baryon and antibaryon in each pair is distributed uniformly within $|\Delta y| < d$, which emulates the law of *local* baryon conservation. In case of flat rapidity distribution of baryon-antibaryon sources, one may substitute ν_s (15), obtained in the model (ii), into (25) in order to get analytical values of $r_{\Delta N}$ for the numerical model from [24].

When there are multiple types of sources in a system, we may write the “superposition” expression for $r_{\Delta N}$ using (21) as

$$r_{\Delta N} = 1 - \sum_{i=1}^{M_s} \alpha^i \nu_s^i. \quad (27)$$

IV. HIGHER-ORDER CUMULANTS FROM BALANCE FUNCTION AT LHC ENERGIES

Ratios of higher-orders cumulants of ΔN distribution to the second cumulant are of great interest to be pre-

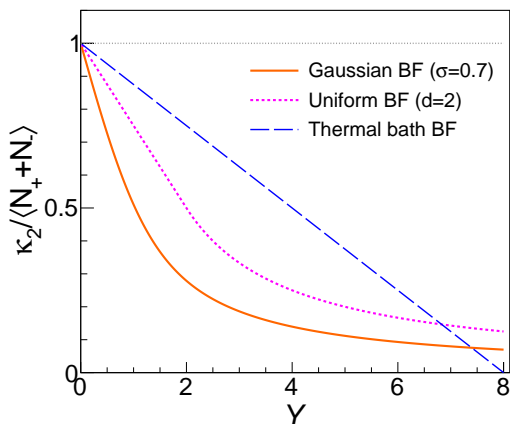


FIG. 4. Ratio of the second cumulant $\kappa_2(\Delta N)$ to the Skellam baseline for Gaussian ($\sigma = 0.7$, solid line), uniform ($d = 2$, dashed line) and “thermal” ($Y_{\max} = 8$, dotted line) balance functions, considered in Section II C.

cisely measured because of their direct connection to theoretically calculated susceptibilities, for example, in the lattice QCD. In collisions of hadrons at the LHC energies, incoming baryonic and electric charges in final state are found to be outside the mid-rapidity acceptance, and practically all opposite-charge pairs at mid-rapidity there are produced in some local processes, in particular, from resonance decays or in fragmentation of quark-gluon strings. In this part of the paper, it is investigated how the local production of particle-antiparticle pairs, characterized by the balance function, is reflected on the higher-order cumulants of net-charge distributions.

A. Cumulants for composition of sources

Suppose that a system, produced in each event, consists of sources that emit particles independently, a number of sources N_S fluctuates event-by-event, and each source is characterized by an (extensive) quantity x , so that the total sum from all the sources in each event is $X = \sum_{i=1}^{N_S} x_i$. In this case, cumulants κ_r of order r of X -distribution could be expressed through a combination of cumulants k_q ($q = 1, \dots, r$) of the x -distribution of a single source and cumulants² K_p ($p = 1, \dots, r$) of the distribution of the number of sources N_S . Such derivations can be performed via moment generating function $M_X(t) = [M_x(t)]^{N_S}$, see [21] and also the Appendix, where expressions for the cumulants up to 8th order are provided.

Putting this into the context of net-charge fluctuations, we set $x = \Delta n$ for a net-charge of the single source and $X = \Delta N$ for the overall net-charge. The second cumulant of the ΔN distribution decomposes then as [21]

$$\kappa_2(\Delta N) = k_2(\Delta n)\langle N_S \rangle + \langle \Delta n \rangle^2 K_2(N_S). \quad (28)$$

It can be seen, that the second cumulant $\kappa_2(\Delta N)$ depends on the fluctuations in number of sources through $K_2(N_S)$ term (the variance of N_S). At this point, we take into account that at the LHC energies $\langle \Delta N \rangle \approx 0$, and it is assumed that the same holds also for sources, $\langle \Delta n \rangle \approx 0$, therefore (28) simplifies to just

$$\kappa_2(\Delta N) = k_2(\Delta n)\langle N_S \rangle. \quad (29)$$

Note, that dependence on the volume fluctuations has gone. The Skellam baseline for a system of sources is

$$\langle N^+ \rangle + \langle N^- \rangle = (\langle n^+ \rangle + \langle n^- \rangle)\langle N_S \rangle, \quad (30)$$

² Different notations for cumulants (κ , k and K) serve only for better visual distinction which distribution they are referred to. The first cumulant κ_1 is just the mean value of X , the second and third cumulants coincide with the 2nd and 3rd central moments, in particular, κ_2 is the variance of X . For higher orders, relations between cumulants and moments are more complicated.

where n^+ and n^- are multiplicities from a single source within the Y acceptance, so the ratio (23) equals

$$r_{\Delta N} = \frac{\kappa_2(\Delta N)}{\langle N^+ \rangle + \langle N^- \rangle} = \frac{k_2(\Delta n)}{\langle n^+ \rangle + \langle n^- \rangle} (= 1 - \nu_s), \quad (31)$$

and it is essential that it does not depend on volume fluctuations. This is the reason why these fluctuations were not discussed in previous two sections. Note also the connection between $k_2(\Delta n)$ and the ν_s in (31).

The 4th cumulant of ΔN (derived in [21], see also the Appendix), in the case when $\langle \Delta n \rangle = 0$, is decomposed as

$$\kappa_4(\Delta N) = k_4(\Delta n)\langle N_S \rangle + 3k_2^2(\Delta n)K_2(N_S), \quad (32)$$

thus, the ratio of the 4th to the 2nd cumulant reads as

$$\frac{\kappa_4}{\kappa_2}(\Delta N) = \frac{k_4}{k_2}(\Delta n) + 3k_2(\Delta n)\frac{K_2(N_S)}{\langle N_S \rangle}. \quad (33)$$

Note, that in this case the volume fluctuations do not cancel – they contribute via the scaled variance $K_2(N_S)/\langle N_S \rangle$. Similarly, the ratio of the 6th cumulant to the 2nd could be derived (see Appendix):

$$\begin{aligned} \frac{\kappa_6}{\kappa_2}(\Delta N) = \frac{k_4}{k_2} + \left(10\frac{k_3^2}{k_2} + 15k_4 \right) \frac{K_2(N_S)}{\langle N_S \rangle} \\ + 15k_2^2 \frac{K_3(N_S)}{\langle N_S \rangle}, \quad (34) \end{aligned}$$

where the (Δn) argument for the k_q terms is omitted for clarity. It can be seen, that in (34) the contribution from volume fluctuations comes already from the two terms that are proportional to $K_2(N_S)$ and to the third cumulant $K_3(N_S)$. Obtained expressions for the ratios will be used below.

In a case when positive and negative particles from each source are sampled from independent Poisson distributions and if there are no volume fluctuations ($K_2(N_S) = K_3(N_S) = 0$), the ratios (33) and (34) become unity.

B. Particle-antiparticle pairs as sources

Formulae (28)–(34) from previous subsection are valid for any types of sources. Let us now make an additional assumption about the nature of the sources, namely, suppose that each source has some rapidity position and it produces exactly one *particle-antiparticle pair* characterized by some balance function³. Moreover, produced particles either do not interact with particles from other sources or may undergo some effective

(charge-independent) rescattering within the surrounding “medium”. The latter leads only to some modification (widening) of the balance functions of each type of sources, keeping, however, the superposition expressions from Section IID valid. It means that we can consider only an “averaged source” of the system, which is characterized by the balance function averaged over sources of different types according to (18).

For such particle-antiparticle sources, all cumulants k_q of orders $q > 2$ can be expressed via the second-order cumulant $k_2(\Delta n)$. This can be shown by expressing the cumulants through the factorial moments, corresponding relations are provided, for instance, in the appendix of the paper [29]. Indeed, factorial moments are defined as

$$f_{i,j} = \left\langle \frac{n^+!}{(n^+ - i)!} \frac{n^-!}{(n^- - j)!} \right\rangle, \quad (35)$$

and for plus-minus pairs all of them, except $f_{1,0}=\langle n^+ \rangle$, $f_{0,1}=\langle n^- \rangle$ and $f_{1,1}=\langle n^+ n^- \rangle$, vanish, because there could not be more than one positive and one negative particle from such a source registered within an acceptance Y . In this way, using formulae from [29], the fourth cumulant of the net-charge distribution for a single source is expressed through the second cumulant as

$$k_4(\Delta n) = k_2(\Delta n) - 3k_2^2(\Delta n), \quad (36)$$

and the 6th-order cumulant – as

$$k_6(\Delta n) = k_2(\Delta n)[1 - 15k_2(\Delta n) + 30k_2^2(\Delta n)]. \quad (37)$$

Substituting (36) into (33), we get the 4-to-2 cumulant ratio for the full system:

$$\frac{\kappa_4}{\kappa_2}(\Delta N) = 1 + 3k_2(\Delta n) \left(\frac{K_2(N_S)}{\langle N_S \rangle} - 1 \right), \quad (38)$$

and substitution of (37) into (34) gives the 6-to-2 cumulant ratio

$$\begin{aligned} \frac{\kappa_6}{\kappa_2}(\Delta N) = 1 - 15k_2 + 30k_2^2 + \\ + 15k_2(1 - 3k_2)\frac{K_2(N_S)}{\langle N_S \rangle} + 15k_2^2\frac{K_3(N_S)}{\langle N_S \rangle}. \quad (39) \end{aligned}$$

In both relations (38) and (39), the information about the decaying sources is now contained only in $k_2(\Delta n)$, which, in turn, can be expressed by inverting (29):

$$k_2(\Delta n) = \frac{1}{\langle N_S \rangle} \kappa_2(\Delta N). \quad (40)$$

Note also, that for the forth-to-second cumulant ratio one needs to know only the first and the second cumulants ($\langle N_S \rangle$ and $K_2(N_S)$) of the source distribution, while for the sixth-to-second cumulant ratio the $K_3(N_S)$ is required in addition.

³ This differs from a more typical interpretation of a source as a “wounded nucleon”, adopted, for instance, in [21].

C. Relation to measurable quantities

Expression (40) for the second cumulant of the source could be plugged into the cumulant ratios (38) and (39) to get formulae in terms of the measurable quantity $\kappa_2(\Delta N)$ and cumulants of the number of sources N_S . However, before doing this, it is convenient to invoke the quantities that will allow simplification of the final expressions. Namely, the r -th order factorial moment of the distribution of the number of sources N_S is given by

$$F_r(N_S) = \left\langle \frac{N_S!}{(N_S - r)!} \right\rangle, \quad (41)$$

and its scaled version minus unity is

$$R_r(N_S) = \frac{F_r(N_S)}{\langle N_S \rangle^r} - 1, \quad (42)$$

so that

$$R_2(N_S) = \frac{\langle N_S(N_S - 1) \rangle}{\langle N_S \rangle^2} - 1 \quad (43)$$

and

$$R_3(N_S) = \frac{\langle N_S(N_S - 1)(N_S - 2) \rangle}{\langle N_S \rangle^3} - 1. \quad (44)$$

The quantities R_r are “robust” in the following sense: if rapidities of the sources are independently sampled from some distribution, while we observe sources only in a restricted acceptance window Y so that we see on average only a fraction ε of all the sources, then R_r do not depend on ε . It means that the quantities R_r remains the same independently of the acceptance, in which we count the sources. Another property of R_r is that they vanish when N_S has Poisson distribution. These properties are discussed, for instance, in [10] for a particular case of R_2 – the so-called robust variance – in the context of its robustness to efficiency losses: in this case, ε plays a role of particle registration efficiency. Note also that values of R_r could be negative as well as positive.

Using (40), (43) and (44), the cumulant ratios (38) and (39) can be rewritten as

$$\begin{aligned} \frac{\kappa_4}{\kappa_2}(\Delta N) &= 1 + 3 \frac{\kappa_2(\Delta N)}{\langle N_S \rangle} \left(\frac{K_2(N_S)}{\langle N_S \rangle} - 1 \right) = \\ &= 1 + 3\kappa_2(\Delta N)R_2(N_S), \end{aligned} \quad (45)$$

and

$$\begin{aligned} \frac{\kappa_6}{\kappa_2}(\Delta N) &= 1 + 15\kappa_2(\Delta N) \left[(1 - 3\kappa_2(\Delta N))R_2(N_S) + \right. \\ &\quad \left. + \kappa_2(\Delta N)R_3(N_S) \right]. \end{aligned} \quad (46)$$

Taking into account the robustness of R_r mentioned above, it may be noted that, if sources are sampled

from their rapidity distribution independently, it is irrelevant for (45) and (46) in which acceptance we calculate $R_2(N_S)$ and $R_3(N_S)$.

Recall now that, in our interpretation, each source produces an oppositely charged particle pair. Let us make an assumption that we can replace cumulants of source number distribution by the cumulants of number distribution of one of its daughter particles (for example, positive ones⁴): $K_r(N_S) \rightarrow K_r(N^+)$, where N^+ is a number of positive particles measured within the Y acceptance. This assumption is fulfilled if the width of the balance function of a source is significantly narrower than the width of the rapidity distribution of the sources ($\sigma_{BF} \ll \sigma_{N_S}$), in order not to “smear” the source rapidity distribution too much (in this case, a positive particle produced from a source can serve as a “proxy” for the source counting). This is typically true at the LHC energies, where the rapidity distribution is nearly flat at mid-rapidity.

After the replacement $K_r(N_S) \rightarrow K_r(N^+)$, which implies also $R_r(N_S) \rightarrow R_r(N^+)$, the expressions (45) and (46) read as

$$\begin{aligned} \frac{\kappa_4}{\kappa_2}(\Delta N) &= 1 + 3 \frac{\kappa_2(\Delta N)}{\langle N^+ \rangle} \left(\frac{K_2(N^+)}{\langle N^+ \rangle} - 1 \right) = \\ &= 1 + 3\kappa_2(\Delta N)R_2(N^+) \end{aligned} \quad (47)$$

and

$$\begin{aligned} \frac{\kappa_6}{\kappa_2}(\Delta N) &= 1 + 15\kappa_2(\Delta N) \left[(1 - 3\kappa_2(\Delta N))R_2(N^+) + \right. \\ &\quad \left. + \kappa_2(\Delta N)R_3(N^+) \right]. \end{aligned} \quad (48)$$

Thus, with assumptions and approximations done above, in order to calculate the forth-to-second order cumulant ratio it is enough to measure within the Y acceptance the second cumulant $\kappa_2(\Delta N)$ and the second-order robust quantity $R_2(N^+)$, while for the six-to-second order ratio, $R_3(N^+)$ is needed in addition. All the quantities $\kappa_2(\Delta N)$, $R_2(N^+)$ and $R_3(N^+)$ are experimentally measurable⁵.

Values of the cumulant ratios calculated with formulae (47) and (48) could be considered as baselines for experimental measurements of the ratios (instead of, for instance, the Skellam baseline), since the formulae are obtained in the simple but physically motivated model of local charge pair production from sources that are uncorrelated in rapidity and when there is no critical behaviour in the system. Possible signals from critical phenomena

⁴ Equally, we can take $K_r(N^-)$ instead, since they are the same as $K_r(N^+)$ in mid-rapidity region at the LHC energies.

⁵ Recall, that $R_r(N^+)$ are robust to efficiency losses (provided that the efficiency is nearly a constant within the acceptance), so the only quantity that should be corrected for efficiency is $\kappa_2(\Delta N)$.

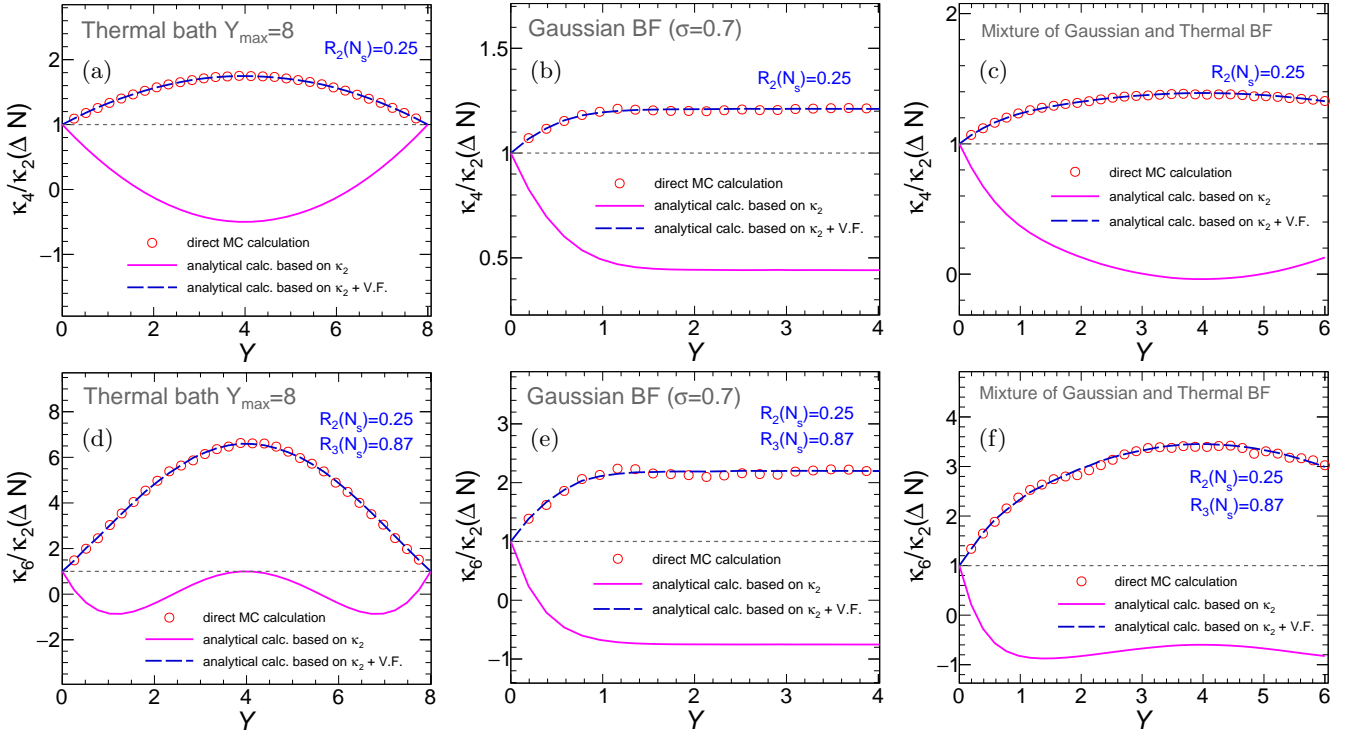


FIG. 5. Ratios κ_4/κ_2 (first row) and κ_6/κ_2 (bottom row) in a toy model with sources that have thermal BF (a, d), Gaussian BF (b, e) and mixture of Gaussian sources (2/3 of all on average) and sources with thermal BF (1/3 on average), panels (c, f). Direct monte-carlo calculations are shown by circles, calculations by (47) and (48) are shown by dashed lines. In all the three cases, number of sources fluctuates with $R_2(N_S) = 0.25$ and $R_3(N_S) = 0.87$. Solid magenta lines represent the ratios for the artificial case when there are no volume fluctuations.

would be indicated by some deviations from these baselines.

Note also, that expressions (47) and (48) could be expressed in terms of ν_s : since $\langle N^+ \rangle = \langle N^- \rangle$, according to (31), we have

$$\kappa_2(\Delta N) = 2\langle N^+ \rangle(1 - \nu_s), \quad (49)$$

and (47) becomes

$$\frac{\kappa_4}{\kappa_2}(\Delta N) = 1 + 6(1 - \nu_s)\langle N^+ \rangle R_2(N^+). \quad (50)$$

A formula for $\kappa_6/\kappa_2(\Delta N)$ can be written in a similar way.

D. Cumulant ratios in simple models

Before using formulae (47) and (48) for studies of realistic events, it is useful to demonstrate behaviour of the cumulant ratios κ_4/κ_2 and κ_6/κ_2 in simple models. From (31) we may get the following relation between the $\kappa_2(\Delta n)$ of a source and ν_s :

$$\kappa_2(\Delta n) = 2\langle n \rangle(1 - \nu_s), \quad (51)$$

where $2\langle n \rangle$ is an average multiplicity from a single source within the Y acceptance ($\langle n \rangle \equiv \langle n^+ \rangle = \langle n^- \rangle$). The

expression (38) becomes

$$\frac{\kappa_4}{\kappa_2}(\Delta N) = 1 + 6\langle n \rangle(1 - \nu_s) \left(\frac{K_2(N_S)}{\langle N_S \rangle} - 1 \right). \quad (52)$$

If we now recall the model (iii) of the “thermal bath”, discussed earlier, where $\nu_s = Y/Y_{\max}$ and $\langle n \rangle = Y/Y_{\max}$ (since both positive and negative particles are thermalized within the Y_{\max} acceptance), and thus $\langle n \rangle = \nu_s$, (52) reads as

$$\frac{\kappa_4}{\kappa_2}(\Delta N) = 1 + 6\nu_s(1 - \nu_s) \left(\frac{K_2(N_S)}{\langle N_S \rangle} - 1 \right). \quad (53)$$

In particular, when volume fluctuations are absent, (53) becomes

$$\frac{\kappa_4}{\kappa_2}(\Delta N) = 1 - 6\nu_s(1 - \nu_s). \quad (54)$$

This result is similar to what was obtained in [30] within the Canonical Ensemble formulation of statistical mechanics (and ν_s corresponds to the acceptance factor α considered in [21, 23, 30]). In a similar way, it can be shown that the sixth-to-second order cumulant ratio (39) for the “thermal bath” model with no volume fluctuations equals

$$\frac{\kappa_6}{\kappa_2}(\Delta N) = 1 - 30\nu_s(1 - \nu_s)[1 - 4\nu_s(1 - \nu_s)]. \quad (55)$$

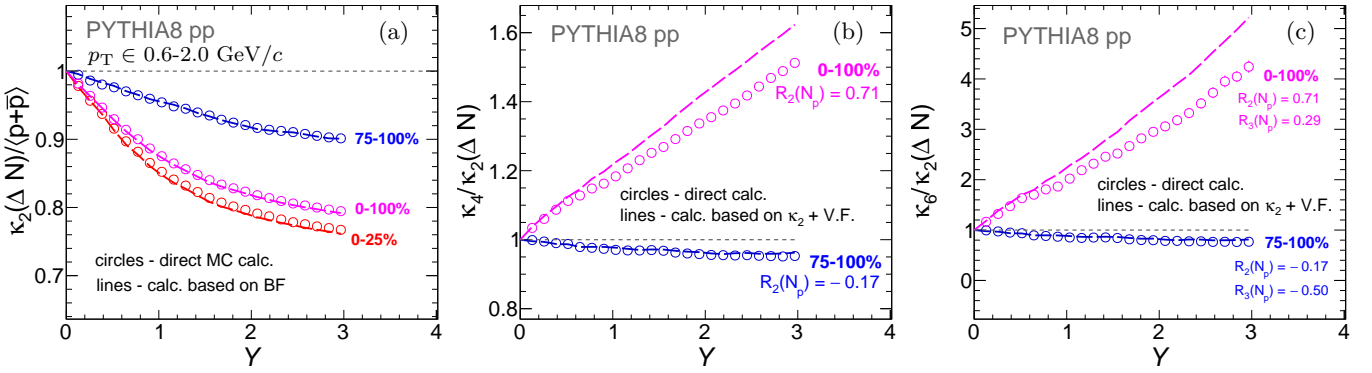


FIG. 6. Dependence of net-proton fluctuations in PYTHIA8 (pp, $\sqrt{s} = 2.76$ TeV, $p_T \in (0.6, 2.0)$ GeV/c) on the size of the rapidity acceptance, in terms of (a) ratio of $\kappa_2(\Delta N)$ to the Skellam baseline $\langle N_p \rangle + \langle N_{\bar{p}} \rangle$, (b) net-proton κ_4/κ_2 and (c) κ_6/κ_2 ratios, in several multiplicity classes. Direct calculations are shown by circles, analytical calculations – by dashed lines.

Dependence of the cumulant ratios κ_4/κ_2 and κ_6/κ_2 on the size of the acceptance Y , calculated with (54) and (55), is shown in Figure 5 in panels (a) and (d) with solid magenta lines. To emulate a more realistic case, events with volume fluctuations (i.e. with fluctuations of N_S), where each source is characterized by the “thermal” balance function, were generated in a monte-carlo model. Circle markers in Figure 5 correspond to direct analysis of the monte-carlo events, while the dashed lines stand for calculations “as in a real experiment” with (47) and (48). An exact correspondence, expected by construction, could be seen.

In case of Gaussian balance function, corresponding results could be obtained by plugging ν_s given by (13) into (51). Analytical calculations for the case with no volume fluctuations are shown in Figure 5 (b, e) by magenta lines, markers stand for values from direct analysis of the toy events with volume fluctuations, calculations with (47) and (48) – by dashed lines. Panels (c) and (f) show the case of a mixture of the sources, namely, when a source with probability 1/3 has the “thermal” balance function and with probability 2/3 – Gaussian BF. It can be seen that calculations with (47) and (48) agree to the values from the direct analysis of toy events.

E. Application to realistic models

Validity of the assumptions about charged pair production, which led to relations (47) and (48) for the cumulant ratios, can be put into test with more realistic events simulated in monte-carlo generators. As an example, net-proton fluctuations ($\Delta N = N_p - N_{\bar{p}}$) in PYTHIA8 [31] in pp collisions at $\sqrt{s} = 2.76$ TeV are considered. Protons and antiprotons are selected within a mid-rapidity range $y \in (-1.5, 1.5)$, additionally, the transverse momentum (p_T) cuts 0.6-2.0 GeV/c are applied, which are similar to the cuts used in net-proton fluctuation analysis in ALICE [14] and STAR [17] experiments.

Dependences of cumulant ratios on the size of the ac-

ceptance window Y are shown in Figure 6. Panel (a) demonstrates the ratio of the second cumulant to the Skellam baseline calculated directly (circles) and through the balance function using formula (26) (lines). As expected, agreement between the values is observed. Results in magenta color correspond to all events (0-100%, “minimum bias”), in red – to events with high particle multiplicity (0-25% of multiplicity percentiles) and in blue – to the lowest multiplicities (75-100%). The difference in the three curves indicates an evolution of the balance function and its integral with event multiplicity (the integral grows in high-multiplicity events). Recall that volume fluctuations does not play any role here.

Panels (b) and (c) of the Figure 6 show, respectively, κ_4/κ_2 and κ_6/κ_2 ratios calculated directly and with expressions (47) and (48). It can be seen that values from minimum-bias events (0-100%, in magenta) are much

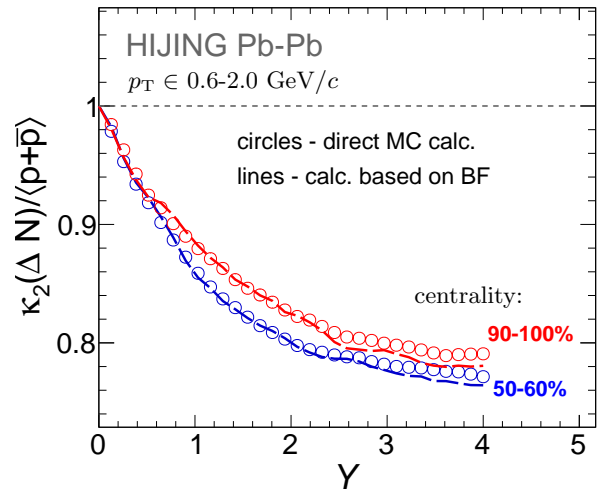


FIG. 7. Ratio of the $\kappa_2(\Delta N)$ of the net-proton distribution to the Skellam baseline in HIJING (Pb-Pb events at $\sqrt{s_{NN}} = 2.76$ TeV). Two centrality classes are shown. Circles – direct calculation, lines – calculation via balance function using (26).

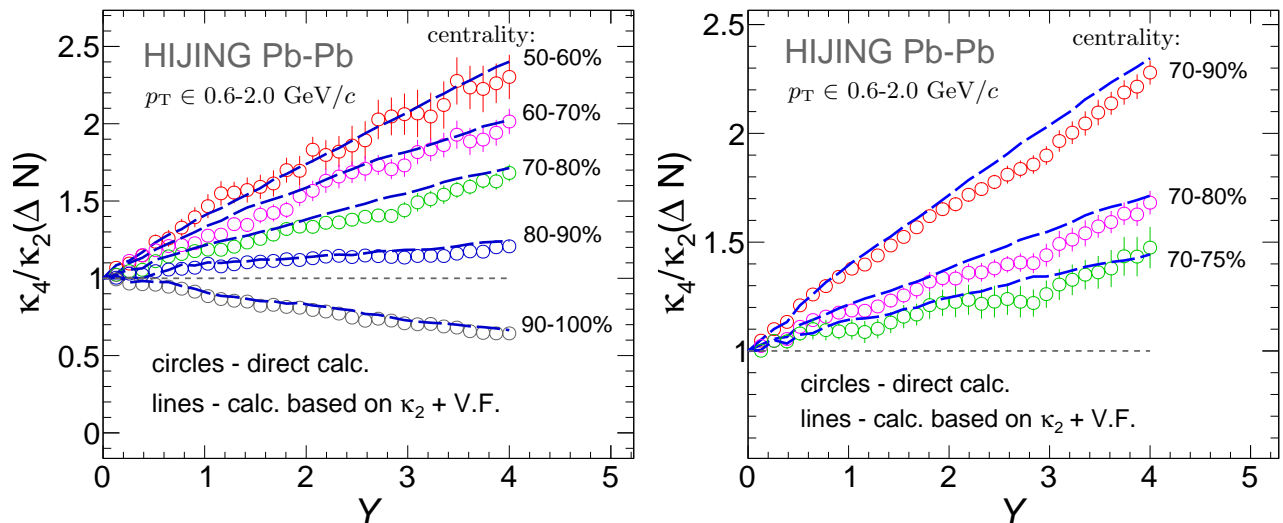


FIG. 8. Dependence on the size of the rapidity acceptance of the net-proton κ_4/κ_2 ratio in HIJING in Pb-Pb events at $\sqrt{s_{NN}} = 2.76$ TeV. Direct calculations are shown by circles, analytical calculations with (47) – by dashed lines. Panel (a) – results in several centrality classes of the class width 10% are shown, (b) – dependence on the width of centrality class (20%, 10% and 5%) is demonstrated.

higher than in a narrower multiplicity class (“peripheral” collisions 75-100%, in blue) due to higher fluctuations in a number of sources. Note, that in PYTHIA, as in any realistic monte-carlo event generator, different kinds of particle emitting sources are present, such as resonances of various species, quark-gluon strings, jets. In the minimum bias case, there is a mixture of events that may significantly differ in terms of spectra, fractions of different resonances, that may produce correlations between number of emitting sources and their balance functions. This violates the assumptions done for derivation of (47) and (48), therefore, in case of minimum-bias (0-100%) events, a visible deviation between the direct and analytical calculations could be seen. At the same time, in the narrow 75-100% multiplicity class a better agreement between the direct and calculated values is observed.

Similar analysis of net-proton fluctuations is performed also in Pb-Pb collisions simulated in HIJING event generator at $\sqrt{s_{NN}} = 2.76$ TeV. Centrality classes were selected using sum of particle multiplicities in symmetric $3 < |\eta| < 5$ ranges, which approximately emulates the way how the centrality is determined in real experiments. Protons and antiprotons were selected in a range $y \in (-2, 2)$. Figure 7 demonstrates the $\kappa_2(\Delta N)$ to Skellam ratio in peripheral (90-100%) and non-peripheral (50-60%) classes. Again, direct and BF-based calculations are in agreement. It could be seen also that results in the two centrality classes are very close to each other. In fact, it was checked that in all non-peripheral classes in a range 0-90% values of κ_2 /Skellam ratio at a given Y are almost identical, because there are no significant collective effects in HIJING and thus the balance function does not evolve with centrality.

Figure 8 (a) shows the κ_4/κ_2 ratios, calculated directly

(circles) and by expression (47) (lines), in several centrality classes of HIJING events⁶. A good agreement between the calculations can be seen in all classes, indicating that the assumption about the plus-minus pairs as nearly independent sources is approximately valid in HIJING, at least for the net-proton fluctuations. Since the balance function (and thus the $\kappa_2/\langle N_p \rangle$ ratio) in all the classes is the same, a change of a line “slope” in different classes in Fig. 8 is determined, according to (47), solely by the $K_2(N_p)/\langle N_p \rangle$ ratio, that is, by the volume fluctuation term. Panel (b) demonstrates a decrease of κ_4/κ_2 values with the width of a centrality class (when the width changes from 20% down to 5%), which is explained by reduction of the volume fluctuations with the narrowing of the class.

It is essential for calculations (and useful in general) to check also the behaviour of the robust quantities R_r within the acceptance, since in Section IV C we assumed that the sources are nearly uncorrelated and thus the R_r values should stay constant as a function of the rapidity acceptance width Y . Figure 9 shows the Y -dependence of the robust variance $R_2(N_p)$ of the number of protons in HIJING in several centrality classes – indeed, the values as a function of Y are stable, indicating that rapidities of protons (number of which is taken as a proxy for a number of proton-antiproton pairs) are almost uncorrelated.

⁶ Available HIJING statistics (about 1.5 mln events) is not enough to get statistically meaningful results for the higher-order κ_6/κ_2 ratio.

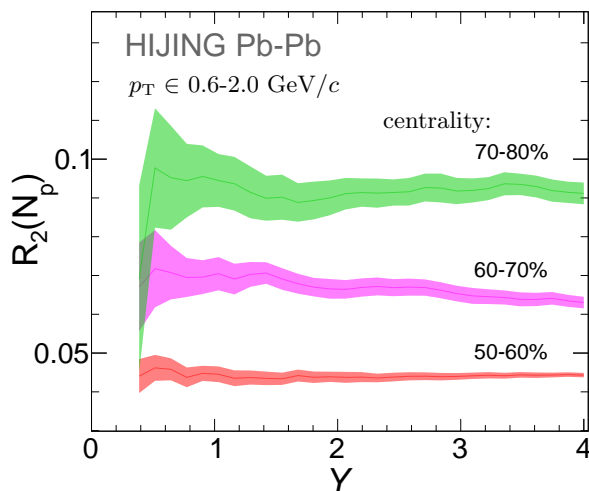


FIG. 9. Robust variance of the number of protons $R_2(N_p)$ as a function of the rapidity acceptance width in three centrality classes in Pb-Pb events from HIJING.

F. Baseline for net-proton κ_4/κ_2 ratio in real data

In order to do an estimation for the κ_4/κ_2 ratio of net-proton fluctuations with expression (47), one needs to know only $\kappa_2(\Delta N)$ and $R_2(N_p)$ within some rapidity acceptance. It is possible to do a prediction for the κ_4/κ_2 ratios for real Pb-Pb events at $\sqrt{s_{NN}} = 2.76$ TeV basing on ALICE results published in [14], namely, taking ratios $r_1 = \kappa_2(\Delta N)/\langle N_p + N_{\bar{p}} \rangle = \kappa_2(\Delta N)/(2\langle N_p \rangle)$ and $r_2 = K_2(N_p)/\langle N_p \rangle$ shown in Figure 1 in this publication for each centrality class. Using these notations, the equality

(47) can be rewritten as

$$\frac{\kappa_4}{\kappa_2}(\Delta N) = 1 + 6r_1(r_2 - 1). \quad (56)$$

Markers in Figure 10 show κ_4/κ_2 ratios estimated by (56) in several centrality classes. The first two classes that correspond to central collisions have a width of 5% (0-5% and 5-10%), while the width of other classes is 10%. Since in narrower classes the volume fluctuations are suppressed, the first two red points are lower than other points. Corresponding direct analysis of HIJING events performed with the same kinematic cuts (a dashed line) shows a trend that is similar to the prediction for data. An increase towards central collisions is explained by a rise in the volume fluctuations with centrality. Note that the rapidity ranges used for centrality selection in HIJING and in real data slightly differ.

The points in Figure 10 may be considered as a baseline for direct calculations of the κ_4/κ_2 ratios in data, within the same centrality classes as in [14]. We might expect deviations from these values in case if the assumptions, done about the sources in order to obtain (47) and then (56), are violated, namely, if the protons (which play a role of sources in this approach) are highly correlated and/or when protons and antiprotons, produced locally, experience subsequent charge-dependent interactions at late stages of the system evolution. Deviation from the baseline may be also a sign of some critical phenomena. Therefore, it seems interesting to perform this analysis also in narrower centrality bins, which would lead to smaller volume fluctuations, and check the validity of the formula (47) by comparing the calculated values with the results of the direct analysis.

V. SUMMARY

In this paper, connections between the balance function and several integrated observables used in studies of net-charge fluctuations were discussed. In the first part of the paper, relation between the balance function integral and the scaled version of the ν_{dyn} observable (ν_s), that holds at LHC energies, was recalled. A difference between balance function definitions that are used in various experiments was highlighted, and the role of the acceptance correction factor in the interpretation of the balance function and its integral was emphasized. For several illustrative cases of the balance function shapes, analytical dependences of the balance function integral and the scaled ν_{dyn} on the size of the acceptance window were given. In case of a system with different types of neutral particle-antiparticle sources, simple superposition formulae for balance function, its integral and scaled ν_{dyn} were provided.

In the second part of the paper, relations for higher-order cumulants (κ_4/κ_2 and κ_6/κ_2) of net-charge distribution are derived under the assumption that particle-antiparticle pairs are produced in local processes from

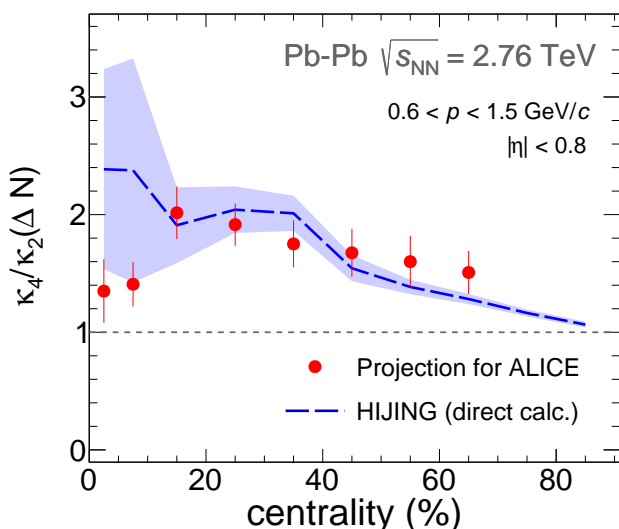


FIG. 10. Projection for the κ_4/κ_2 ratio of net-proton fluctuations in Pb-Pb collisions at $\sqrt{s_{NN}} = 2.76$ TeV based on ALICE results for the second-order cumulants [14]. Line shows results of direct analysis of HIJING events with the same kinematic cuts for particles.

sources that are nearly uncorrelated in rapidity. It turns out that for calculation of these ratios it is enough to know the second moment of net-charge distribution (connected to the balance function and the scaled ν_{dyn}) and low-order cumulants of number of positive (or negative) particles within the acceptance. It was demonstrated that in realistic events from PYTHIA and HIJING event generators the values, obtained with the derived expressions, match with direct calculations of the cumulant ratios. Finally, using the obtained expressions and basing on available experimental results on the second cumulants, a prediction for the κ_4/κ_2 ratio in Pb-Pb collisions at $\sqrt{s_{NN}}=2.76$ TeV has been done for centrality classes of the width 10% (5% for the two most central classes). It would be interesting to compare direct and analytical calculations of the ratios in narrower centrality classes as well, since in this case the volume fluctuations will be suppressed. Values of the κ_4/κ_2 and κ_6/κ_2 ratios, obtained with the derived expressions, could be considered as baselines for direct calculations, since discrepancies may indicate signs of some critical behaviour present in the system.

ACKNOWLEDGEMENTS

The author would like to thank Vladimir Vechernin for fruitful discussions. This work is supported by the Russian Science Foundation, grant 17-72-20045.

Appendix: Expressions for cumulants in models with multiple sources

In this Appendix, analytical formulae for cumulants up to 8th order are derived in a model with a superposition

of sources. Obtained results are used in the main text in Section IV A.

If a number of sources N_S fluctuates event-by-event, and each source is characterized by an extensive quantity x , so that the total sum from all the sources in each event is $X = \sum_{i=1}^{N_S} x_i$, then cumulants κ_r of order r of X -distribution can be expressed through a combination of cumulants k_q ($q = 1, \dots, r$) of the x -distribution for a single source and cumulants K_p ($p = 1, \dots, r$) of the distribution of the number of sources N_S using moment generating function $M_X(t) = [M_x(t)]^{N_S}$, in a way it is done in [21]. Recall, that different notations for cumulants (κ , k and K) serve only for the purpose of better visual distinction. The first four cumulants of X -distribution are expressed as follows:

$$\kappa_1 = k_1 K_1, \quad (\text{A.1})$$

$$\kappa_2 = k_2 K_1 + k_1^2 K_2, \quad (\text{A.2})$$

$$\kappa_3 = k_3 K_1 + 3k_2 k_1 K_2 + k_1^3 K_3, \quad (\text{A.3})$$

$$\kappa_4 = k_4 K_1 + (3k_2^2 + 4k_1 k_3) K_2 + 6k_2 k_1^2 K_3 + k_1^4 K_4. \quad (\text{A.4})$$

Formulae (A.1)–(A.4) were obtained in [21]. Following the same strategy, we can write down expressions for higher orders, which are given below up to order 8:

$$\kappa_5 = k_5 K_1 + 5(2k_2 k_3 + k_1 k_4) K_2 + 5(3k_2^2 k_1 + 2k_1^2 k_3) K_3 + 10k_2 k_1^3 K_4 + k_1^5 K_5, \quad (\text{A.5})$$

$$\kappa_6 = k_6 K_1 + (10k_3^2 + 15k_2 k_4 + 6k_1 k_5) K_2 + (15k_2^3 + 15k_4 k_1^2 + 60k_2 k_3 k_1) K_3 + (45k_2^2 k_1^3 + 20k_3 k_1^3) K_4 + 15k_2 k_1^4 K_5 + k_1^6 K_6, \quad (\text{A.6})$$

$$\kappa_7 = k_7 K_1 + 7(5k_3 k_4 + 3k_2 k_5 + k_1 k_6) K_2 + (21k_5 k_1^2 + 70k_3^2 k_1 + 105k_2 k_4 k_1 + 105k_2^2 k_3) K_3 + (35k_4 k_1^3 + 210k_2 k_3 k_1^2 + 105k_2^3 k_1) K_4 + (105k_2^2 k_1^3 + 35k_3 k_1^4) K_5 + 21k_2 k_1^5 K_6 + k_1^7 K_7, \quad (\text{A.7})$$

$$\kappa_8 = k_8 K_1 + (35k_4^2 + 56k_3 k_5 + 28k_2 k_6 + 8k_1 k_7) K_2 + (280k_3 k_4 k_1 + 168k_2 k_5 k_1 + 280k_2 k_3^2 + 210k_2^2 k_4 + 28k_6 k_1^2) K_3 + (56k_5 k_1^3 + 280k_3^2 k_1^2 + 420k_2 k_4 k_1^2 + 840k_2^2 k_3 k_1 + 105k_2^4) K_4 + (70k_4 k_1^4 + 560k_2 k_3 k_1^3 + 420k_2^3 k_1^2) K_5 + (56k_3 k_1^5 + 210k_2^2 k_1^4) K_6 + 28k_2 k_1^6 K_7 + k_1^8 K_8, \quad (\text{A.8})$$

At the LHC energies, in the context of net-charge fluctuations,

$k_1 = \langle \Delta n \rangle = 0$, so equations (A.1)–(A.8) sim-

plify:

$$\kappa_1 = 0, \quad (\text{A.9})$$

$$\kappa_2 = k_2 K_1, \quad (\text{A.10})$$

$$\kappa_3 = k_3 K_1, \quad (\text{A.11})$$

$$\kappa_4 = k_4 K_1 + 3k_2^2 K_2, \quad (\text{A.12})$$

$$\kappa_5 = k_5 K_1 + 10k_2 k_3 K_2, \quad (\text{A.13})$$

$$\kappa_6 = k_6 K_1 + (10k_3^2 + 15k_2 k_4) K_2 + 15k_2^3 K_3, \quad (\text{A.14})$$

$$\kappa_7 = k_7 K_1 + 7(5k_3 k_4 + 3k_2 k_5) K_2 + 105k_3 k_2^2 K_3, \quad (\text{A.15})$$

$$\kappa_8 = k_8 K_1 + (35k_4^2 + 56k_3 k_5 + 28k_2 k_6) K_2 + (210k_4 k_2^2 + 280k_3^2 k_2) K_3 + 105k_2^4 K_4. \quad (\text{A.16})$$

- [1] A. Bazavov *et al.*, *Phys. Rev.* **D85**, 054503 (2012), [arXiv:1111.1710 \[hep-lat\]](#).
- [2] M. A. Stephanov, K. Rajagopal, and E. V. Shuryak, *Phys. Rev.* **D60**, 114028 (1999), [arXiv:hep-ph/9903292 \[hep-ph\]](#).
- [3] M. A. Stephanov, *Non-perturbative quantum chromodynamics. Proceedings, 8th Workshop, Paris, France, June 7-11, 2004*, *Prog. Theor. Phys. Suppl.* **153**, 139 (2004), [*Int. J. Mod. Phys.A*20,4387(2005)], [arXiv:hep-ph/0402115 \[hep-ph\]](#).
- [4] S. A. Bass, P. Danielewicz, and S. Pratt, *Phys. Rev. Lett.* **85**, 2689 (2000), [arXiv:nucl-th/0005044 \[nucl-th\]](#).
- [5] M. M. Aggarwal *et al.* (STAR), *Phys. Rev.* **C82**, 024905 (2010), [arXiv:1005.2307 \[nucl-ex\]](#).
- [6] B. Abelev *et al.* (ALICE), *Phys. Lett.* **B723**, 267 (2013), [arXiv:1301.3756 \[nucl-ex\]](#).
- [7] J. Adam *et al.* (ALICE), *Eur. Phys. J.* **C76**, 86 (2016), [arXiv:1509.07255 \[nucl-ex\]](#).
- [8] J. Pan (ALICE), *Proceedings, 27th International Conference on Ultrarelativistic Nucleus-Nucleus Collisions (Quark Matter 2018): Venice, Italy, May 14-19, 2018*, *Nucl. Phys.* **A982**, 315 (2019), [arXiv:1807.10377 \[nucl-ex\]](#).
- [9] S. Acharya *et al.* (ALICE), *Phys. Rev.* **C100**, 044903 (2019), [arXiv:1805.04422 \[nucl-ex\]](#).
- [10] C. Pruneau, S. Gavin, and S. Voloshin, *Phys. Rev.* **C66**, 044904 (2002), [arXiv:nucl-ex/0204011 \[nucl-ex\]](#).
- [11] B. I. Abelev *et al.* (STAR), *Phys. Rev.* **C79**, 024906 (2009), [arXiv:0807.3269 \[nucl-ex\]](#).
- [12] B. Abelev *et al.* (ALICE), *Phys. Rev. Lett.* **110**, 152301 (2013), [arXiv:1207.6068 \[nucl-ex\]](#).
- [13] S. Acharya *et al.* (ALICE), *Eur. Phys. J.* **C79**, 236 (2019), [arXiv:1712.07929 \[nucl-ex\]](#).
- [14] S. Acharya *et al.* (ALICE), (2019), [arXiv:1910.14396 \[nucl-ex\]](#).
- [15] A. Ohlson (ALICE), *Proceedings, 27th International Conference on Ultrarelativistic Nucleus-Nucleus Collisions (Quark Matter 2018): Venice, Italy, May 14-19, 2018*, *Nucl. Phys.* **A982**, 299 (2019), [arXiv:1901.00744 \[nucl-ex\]](#).
- [16] L. Adamczyk *et al.* (STAR), *Phys. Rev. Lett.* **113**, 092301 (2014), [arXiv:1402.1558 \[nucl-ex\]](#).
- [17] J. Adam *et al.* (STAR), (2020), [arXiv:2001.02852 \[nucl-ex\]](#).
- [18] L. Adamczyk *et al.* (STAR), *Phys. Lett.* **B785**, 551 (2018), [arXiv:1709.00773 \[nucl-ex\]](#).
- [19] S. Jeon and S. Pratt, *Phys. Rev.* **C65**, 044902 (2002), [arXiv:hep-ph/0110043 \[hep-ph\]](#).
- [20] C. A. Pruneau, *Phys. Rev.* **C100**, 034905 (2019), [arXiv:1903.04591 \[nucl-th\]](#).
- [21] P. Braun-Munzinger, A. Rustamov, and J. Stachel, *Proceedings, 27th International Conference on Ultrarelativistic Nucleus-Nucleus Collisions (Quark Matter 2018): Venice, Italy, May 14-19, 2018*, *Nucl. Phys.* **A982**, 307 (2019), [arXiv:1807.08927 \[nucl-th\]](#).
- [22] T. Sugiura, T. Nonaka, and S. Esumi, *Phys. Rev.* **C100**, 044904 (2019), [arXiv:1903.02314 \[nucl-th\]](#).
- [23] A. Bzdak, V. Koch, and V. Skokov, *Phys. Rev.* **C87**, 014901 (2013), [arXiv:1203.4529 \[hep-ph\]](#).
- [24] P. Braun-Munzinger, A. Rustamov, and J. Stachel, (2019), [arXiv:1907.03032 \[nucl-th\]](#).
- [25] M. I. Gorenstein and M. Gazdzicki, *Phys. Rev.* **C84**, 014904 (2011), [arXiv:1101.4865 \[nucl-th\]](#).
- [26] V. Vechernin and E. Andronov, *Proceedings, 7th International Conference on New Frontiers in Physics (ICNFP 2018): Kolymbari, Crete, Greece, July 4-12, 2018*, *Universe* **5**, 15 (2019).
- [27] I. Altsybeev, *Proceedings, 25th Cracow Epiphany Conference on Advances in Heavy Ion Physics (Epiphany 2019): Cracow, Poland, January 8-11, 2019*, *Acta Phys. Polon.* **B50**, 981 (2019), [arXiv:1903.10085 \[nucl-th\]](#).
- [28] S. N. Belokurova and V. V. Vechernin, *Theor. Math. Phys.* **200**, 1094 (2019), [*Teor. Mat. Fiz.*200,no.2,195(2019)].
- [29] A. Bzdak and V. Koch, *Phys. Rev.* **C86**, 044904 (2012), [arXiv:1206.4286 \[nucl-th\]](#).
- [30] P. Braun-Munzinger, A. Rustamov, and J. Stachel, *Proceedings, 27th International Conference on Ultrarelativistic Nucleus-Nucleus Collisions (Quark Matter 2018): Venice, Italy, May 14-19, 2018*, *Nucl. Phys.* **A982**, 307

(2019), [arXiv:1807.08927 \[nucl-th\]](#).

[31] T. Sjostrand, S. Mrenna, and P. Z. Skands, *JHEP* **05**, 026 (2006), [arXiv:hep-ph/0603175 \[hep-ph\]](#).